Tracer Tests in a Fractured Dolomite:

2. Controls on Mass-Recovery Rates for a Single-Porosity, Heterogeneous Conceptualization

Susan J. Altman
Lucy C. Meigs
Sandia National Laboratories
Geohydrology Department
P.O. Box 5800 MS0735
Albuquerque, NM 87185-0735
email: sjaltma@sandia.gov

Toya L. Jones
Duke Engineering and Services, Inc.
9111 Research Boulevard
Austin, TX 78758

Submitted to Water Resource Research, December 1998

DISCLAIMER

Abstract

A single-well injection-withdrawal (SWIW) test is evaluated as a tool to differentiate between single- and double-porosity conceptualizations of a system. Results from single-porosity simulations incorporating plume drift are also compared to observed data from a recent series of SWIW tests conducted in a fractured dolomite unit, for which a double-porosity conceptualization has been proposed. We evaluate the difficulty of differentiating the response for a double-porosity conceptualization from that for a heterogeneous, single-porosity conceptualization incorporating plume drift. Results of sensitivity studies on multiple, stochastically generated, heterogeneous transmissivity fields indicate that to simulate extremely slow mass-recovery rates for a SWIW test with a single-porosity conceptualization, the following conditions must be present: plume drift, extreme heterogeneities (high $\sigma \ln T$), and an unusual configuration of the high and low transmissivity regions relative to the well location. A compilation of existing data suggests that the high degree of heterogeneity necessary is rare at the SWIW test scale. The observed data from the SWIW tracer tests cannot be matched to numerical simulation results when a single-porosity conceptualization is assumed. A signature of significant drift is less than 100% mass recovery with a zero derivative with respect to time of the late-time normalized cumulative mass curve indicating mass transported outside the capture zone of the withdrawal well. To minimize the risk of misinterpretation, an important design feature for SWIW tests is the collection of late-time data so that percent total mass recovery can be calculated.

1. Introduction

In modeling transport of solutes in the subsurface, the identification of when a single- or double porosity conceptualization is needed is important. Numerical modeling studies by *Tsang* [1995] suggest that SWIW tracer tests may be an excellent method for distinguishing between double- and single-porosity conceptualizations. However, recent numerical modeling by *Lessoff and Konikow* [1997] suggests that it may be difficult to differentiate the response for a double-porosity conceptualization from the response for a heterogeneous, single-porosity conceptualization incorporating plume drift. This paper presents numerical modeling results performed in conjunction with the first series of SWIW tracer tests designed, in part, to evaluate the hypothesis that SWIW tests are an effective tool for distinguishing between single- and double-porosity conceptualizations [*Meigs and Beauheim*, this issue]. In addition, the tracer test results are used to evaluate the importance of matrix diffusion in a fractured dolomite in southeastern New Mexico.

Matrix diffusion is recognized as a potentially important process in the transport of solutes in the subsurface. For example, the *National Research Council* [1994, p. 2-3] identified diffusion of solutes into "immobile" regions of the subsurface as one of the key technical reasons leading to difficulty in predicting and accomplishing aquifer restoration. The transfer of mass via diffusion from high permeability, advection-dominated domains into and out of low permeability, diffusion-dominated domains can significantly affect contaminant migration at any scale. In addition, matrix diffusion can also be an important process in providing access to sorption sites within the matrix [*Ball and Roberts*, 1991; *Wood et al.*, 1990]. Thus, in modeling transport of solutes in the subsurface, recognition of the role of diffusion is important. Field tracer tests can be used to

provide valuable insight on transport processes such as matrix diffusion [e.g. *Volckaert and Gautschi*, 1997; *Moench*, 1995; *Jones et al.*, 1992; *Abelin et al.*, 1991].

For SWIW tracer tests, also referred to as huff-puff or push-pull tests, a single well is used to both inject and withdraw a solute into and out of an aquifer. Frequently, the tests include a resting phase between injection and withdrawal to allow for tracer interaction with the aquifer fluids or materials. SWIW tests have been conducted to measure residual oil saturation [*Seetharam and Deans*; 1989, *Majoros and Deans*, 1980; *Tomich et al.*, 1973], investigate microbial metabolic activities [*Istok et al.*, 1997], and measure advective groundwater velocity [*Leap and Kaplan*, 1988].

Tsang [1995] conducted several numerical simulations for different types of tracer tests to determine which test(s) could be used to evaluate the importance of matrix diffusion. *Tsang* [1995] found that if tracer is injected into one well and recovered from a second, heterogeneity may cause gradual mass recovery, making it difficult to differentiate between single-porosity and double-porosity conceptualizations. Simulations of SWIW tracer tests, in contrast, had significantly faster mass recovery for a single-porosity conceptualization as compared to a double-porosity conceptualization. The dramatically different recovery curves for the two different conceptualizations suggest that the SWIW tests can be used to evaluate the importance of matrix diffusion. *Tsang* [1995] also noted that the late-time slope of time (t) versus concentration on a log-log plot is always -1.5 for the double-porosity simulations. Thus, heterogeneity does not change the asymptotic $t^{-1.5}$ dependence in the analytic solution for double-porosity transport [*Heer and Hadermann*, 1994; *Meigs et al.*, in review]. Tsang's work suggests that a -1.5 slope in recovery curves for a SWIW test may be an additional indication of matrix diffusion.

Recent numerical modeling of SWIW tracer tests by *Lessoff and Konikow* [1997] suggests that plume drift, resulting from an ambient flow field, may make it difficult to differentiate the response for a double-porosity conceptualization from the response for a heterogeneous, single-porosity conceptualization. Plume drift during the resting phase can cause the transport pathways to no longer be reversible. *Lessoff and Konikow* [1997] created 90 highly heterogeneous transmissivity fields and simulated the early time (less than 200 hours) transport for a SWIW test with a single-porosity conceptualization incorporating drift. They describe a single-porosity simulation in which, during the resting phase, the plume drifts into a low-transmissivity area located downgradient of the well. Once withdrawal pumping begins, tracer recovery from this lower transmissivity area is slow and the recovered tracer is diluted by fresh water from areas of higher transmissivity. The simulations by *Lessoff and Konikow* [1997] suggest that, under some conditions, regional drift may make it difficult to evaluate whether a single-porosity or a double-porosity conceptualization of the system is appropriate. Thus, given slow mass-recovery rates observed from a SWIW test, an important alternative to the double-porosity conceptualization is a single-porosity conceptualization in a heterogeneous system with plume drift.

In this study, two sets of heterogeneous single-porosity simulations of SWIW tracer tests are conducted. The objective of the first set of simulations, referred to as the sensitivity studies, is to evaluate the conditions that can lead to gradual mass recovery with a single-porosity conceptualization. The relative importance of factors influencing mass-recovery rates (degree of heterogeneity and the amount of drift) and the physical controls on drift (regional gradient, resting-phase duration, porosity) are explored. The objective of the second set, the WIPP-specific simulations, is to evaluate data from recent SWIW tracer tests conducted in a fractured dolomite

[*Meigs and Beauheim*, this issue] and assess the possibility of ruling out a single-porosity conceptualization for this system.

2. WIPP Site Data and Test Design

A series of SWIW and multi-well convergent flow (MWCF) tracer tests were performed in the Culebra Dolomite Member of the Rustler Formation as part of the site characterization of the Waste Isolation Pilot Plant (WIPP). The WIPP site is the U. S. Department of Energy's deep geologic repository for transuranic nuclear waste located in southeastern New Mexico (Figure 1). Background on the motivation for and objectives of the tracer tests is described in *Meigs and Beauheim* [this issue]. Additional interpretations of the SWIW tests and interpretations of the MWCF tests are presented in *Haggerty et al.* [this issue] and *McKenna et al.* [this issue], respectively.

SWIW tracer tests were conducted at two multiple-well sites, or hydropads, designated as H-11 and H-19 (Figure 1). The SWIW tracer tests consisted of 1) tracer solution injection, 2) chaser injection, 3) a resting phase of approximately 18 hours, and 4) withdrawal and collection of samples. Fluoro- and chlorobenzoic acids were used as non-sorbing tracers [*Farnham et al.*, in review; *Meigs et al.*, in review]. The chaser was composed of either Culebra brine or a second slug of tracer followed by Culebra brine. The well was pumped until the tracer concentrations were close to or below detection levels (26-50 days). For more details of the SWIW tests and observed tracer recoveries, see Table 2 and Figures 6 and 7 in *Meigs and Beauheim* [this issue]. For all plots, the concentration and cumulative mass have been normalized to the injected concentration.

The Culebra is a 7-m-thick, highly fractured dolomite located approximately 440 m above the WIPP repository and 190 to 230 m below the ground surface within the WIPP site boundaries. The transmissive portion of the Culebra is estimated at 4.4 m thick at the H-11 and H-19 hydropads. This thickness is based on hydraulic testing [*Beauheim et al.*, 1997; *Mercer and Orr*, 1979], geologic mapping [*Holt and Powers*, 1990], and MWCF tracer test results [*Meigs and Beauheim*, this issue]. This portion of the Culebra can be considered as a confined layer, being underlain by mudstone with an expected transmissivity orders of magnitude lower than that of the Culebra [*Beauheim*, 1987] and overlain by a significantly less transmissive portion of the Culebra. Analysis of hydraulic tests at H-19 showed little to no hydraulic anisotropy in the horizontal plane in the Culebra [*Beauheim and Ruskauff*, 1998]. For a more complete description of the Culebra lithologies and conceptualizations, see *Holt* [1997] and *Meigs and Beauheim* [this issue].

Although there have been numerous hydraulic tests in the vicinity of the WIPP site, relatively little information on the spatial structure of transmissivity at the hydropad scale (tens of meters) is available. The dependence of transmissivity on scale [*Clauser*, 1992; *Gelhar et al.*, 1992] makes it difficult to evaluate the transmissivity distribution for a given location. Data from the Culebra hydraulic tests were compiled and the standard deviation of the natural logarithm of transmissivity was calculated to be 2.1 within the WIPP site boundaries (41.4 km^2) [*Meigs et al.*, in review]. Because this is the standard deviation of measurements over a scale much larger than the hydropad scale (kilometers versus tens of meters) a value of 2.1 is likely an overestimate of σ_{lnT} for the scale of the tracer tests.

3. Numerical Simulations

The simulations described in this paper can be grouped into two categories: sensitivity studies and WIPP-specific studies. The objective of the sensitivity studies is to gain insight into the signature of drift on SWIW recovery curves generated with a single-porosity conceptualization. The purpose of the WIPP-specific simulations is to determine whether the observed tracer test data can be match with a heterogeneous, single-porosity conceptualization. These simulations also provide additional insight by testing the knowledge gained from the sensitivity studies on an example, field problem. For both sets of simulations, numerous, equally plausible, heterogeneous transmissivity (T) fields are generated. Particle tracking is used to model transient advective transport in steady-state flow fields generated using a finite difference approach.

3.1 Approach to representing heterogeneity

For the purposes of this study, the transmissive portion of the Culebra is assumed to be homogeneous in the vertical direction (two-dimensional approximation). This assumption is appropriate because 1) simulations are used for comparative purposes and 2) uncertainty in other parameters and how the uncertainties are handled make the effects of this assumption minimal. Based on extensive hydraulic testing conducted at five hydropads at the WIPP site, including H-11 and H-19 [*Beauheim and Ruskauff*, 1998], the Culebra fractures appear to have a high enough density and be well enough connected to be reasonably approximated by a heterogeneous stochastic continuum for advective transport.

The heterogeneous transmissivity fields are created using sequential simulation algorithms as described in *Deutsch and Journel* [1998]. Generation of transmissivity fields utilizes a

spherical model of spatial correlation with isotropic correlation lengths and no nugget effect. A grid block size is chosen so that at least 10 blocks comprise each correlation length. Two distributions of lnT are used to create two different conceptual models of the transmissivity distribution. The first conceptualization assumes a Gaussian distribution and uses the Gaussian sequential simulation algorithm (*sgsim*) to generate the fields. The second conceptualization assumes a bimodal distribution of lnT and uses the indicator sequential simulation algorithm (*sisim*). The means and univariate ranges of the Gaussian and bimodal distributions are kept approximately the same (Figure 2). The two peaks of the bimodal distribution differ by approximately two orders of magnitude. These two peaks can be conceptualized as 1) highly transmissive fractures and 2) permeable zones in the rock matix where advection takes place.

In addition to the distribution of lnT (Figure 2), the two algorithms differ in their reproduction of the model of spatial correlation. For the *sgsim* algorithm, the model is reproduced at the median of the Gaussian distribution, and extreme high and low values tend to be poorly correlated. With the *sisim* algorithm, the model is reproduced for each specified centile in the generated random transmissivity fields, thus generating well correlated-structures for transmissivity values throughout the distribution. Gaussian distributions created with both *sgsim* and *sisim* have been compared for simulations of MWCF tracer tests [*Meigs et al.*, in review]. In a few simulations, the transmissivity fields created with *sgsim* result in slower mass-recovery rates. The differences in the breakthrough curves are not significant, however, for most realizations.

3.2 Approach to representing flow and transport

Flow and transport in the heterogeneous system is simulated in three steps. First, the heterogeneous transmissivity field is imbedded within a coarser mesh to provide adequate distance between the transport region and the model boundaries. Second, a steady-state flow field is calculated using a finite difference approach for each flow regime (i.e., injection, resting phase, and withdrawal). Third, transient transport in the heterogeneous continuum is simulated by means of particle tracking. The advective flow fields and the particle tracking are simulated with the numerical code THEMM (transport in heterogeneous medium with matrix diffusion) [*Tsang and Tsang*, in review].

Advective transport is modeled on the steady-state flow fields using a particle tracking method. A large number of particles are introduced at the injection well. The residence time (t_w) for the particle within each discretized element is determined based on the element porosity divided by the flux through the element [*Moreno et al.*, 1990]:

$$t_w = \frac{b\phi\Delta x\Delta y}{\frac{1}{2}\sum_j |Q_{ij}|} \tag{1}$$

where b is the thickness [L] of the layer being modeled, ϕ is the porosity [-], Δx and Δy are the grid dimensions [L], and Q_{ij} is the flow rate [L^3/T] through element (i) and the connecting elements (j). Each particle moves through the calculated flow field, and the residence times within each element along the particle paths are summed. Particles are distributed to the neighboring grid cells according to steady-state stream tubes. To minimize numerical dispersion, particles do not diffuse across stream tubes [*Moreno et al.*, 1988]. Arrival times of the particles at the

element containing the withdrawal well are calculated to generate mass-recovery curves. The number of particles in each element at specified times is also calculated in order to determine the spatial distribution of the tracer.

3.3 Model domain and boundary conditions

The model consists of a 4.4-m thick layer extending 634 m in both the x- and y-directions. The central 120 m x 120 m area is heterogeneous with each grid block assigned a different transmissivity value. The remaining portion of the model is homogeneous and assigned a transmissivity equal to the geometric mean value for the heterogeneous region. The model grid blocks are 0.5 m x 0.5 m in the heterogeneous region and increase from 0.5 m to 128 m in the homogeneous region with the largest grid blocks located at the model's outer edge. Solute transport occurs only within the heterogeneous region. Figures of simulation results, such as Figure 4, show only a portion of the heterogeneous domain. The origin referred to in the figures and text is the lower left-hand (southwest) corner of the heterogeneous domain.

Constant-head boundary conditions are set on the four sides of the model domain such that a gradient is induced from the top to the bottom (north to south). The average of the head values assigned at the top and bottom is assigned to the lateral boundaries. Simulations confirm that these lateral boundaries are equivalent to no-flow boundaries and far enough from the inner region to not affect plume dimensions. An internal, constant rate, source/sink term is specified to represent the injection/withdrawal well (located at 60 m, 80 m). A constant injection rate is assigned during injection, a zero rate during the resting phase, and a constant extraction rate during the withdrawal phase. A transmissivity value ten times greater than the maximum transmissivity of the entire field is assigned to the grid block containing the well to represent the

increased conductivity of the well. Because the grid block containing the well is sufficiently small compared to the size and movement of the plume, the increased transmissivity does not significantly affect plume movement.

3.4 Input parameters

The parameter values for the sensitivity studies (Table 1) are based on the Culebra SWIW tests at the H-11 hydropad [*Meigs and Beauheim*, this issue, Table 2]. Parameters for which values were varied for the sensitivity studies fall into one of two groups: 1) parameters that affect the heterogeneity of the system (σ_{lnT}, correlation length, and transmissivity distribution) and 2) parameters that affect drift (porosity, regional gradient, and resting-phase duration). Thirty equally plausible, heterogeneous, random transmissivity-field realizations are used for the sensitivity studies.

For the WIPP-specific simulations, parameter values are chosen based on the test design or, when uncertain, considered to be within realistic bounds for the H-11 and H-19 hydropads (Table 2). When the tracer and chaser injection rates differ, a time-weighted average is used in the simulations. A comparison of this simplified method to the use of two different injection rates shows insignificant differences in simulated mass recovery [*Meigs et al.*, in review]. For parameters that are uncertain (e.g. porosity and hydraulic gradient), a reasonable value leading to the most drift and, as a result, the slowest rate of mass recovery, is selected.

An estimate of porosity is calculated from the MWCF tracer test results at each hydropad assuming direct plug flow between the injection well and the pumping well [*Meigs and Beauheim*, this issue]. The porosity used for the WIPP-specific simulations described here is the minimum

calculated porosity for each hydropad reduced by a factor of five (Table 2). This reduction is made in an effort to minimize simulated mass-recovery rates while maintaining reasonable parameter values: the smaller the porosity, the greater the drift and the slower the mass-recovery rates. The hydraulic gradient at each hydropad is estimated based on five sets of water level measurements taken between September 1996 and July 1997 [*Meigs et al.*, in review]. For each hydropad, the mean plus three times the standard deviation of the five calculated gradients is used as the gradient for the WIPP-specific simulations (Table 2). In estimating bounding values, the gradient is most likely overestimated and the porosity underestimated. This may result in simulations that have more gradual mass recovery than is realistic. However, this method will provide a more rigorous test of whether the field data can be matched with a single-porosity model.

For the WIPP-specific simulations, the transmissivity fields are generated with a Gaussian distribution of lnT. Because mass-recovery rates are expected to decrease with an increase of σ_{lnT}, a conservative value of 2.64 is chosen for the WIPP-specific simulations (Table 2). This value of 2.64 is clearly conservative for the hydropad scale as a standard deviation of 2.1 has been calculated for the larger scale of the entire WIPP site (Table 3). The mean transmissivity values used in the simulations described in this paper are from *Beauheim and Ruskauff* [1998][1] (Table 2). One hundred simulations are conducted for the SWIW test at the H-11 and H-19 hydropads with the longest resting phase. Using the test with the longest resting phase maximizes the effects of regional drift.

[1] The transmissivity value we used for H-11 was actually an early estimation of the transmissivity as part of Beauheim and Ruskauff's [1998] work. The final value published in Beauheim and Ruskauff [1998] is 4.7×10^{-5} m^2/s. The value used is this work (Table 2) is higher, leading to slightly slower mass-recovery rates.

4. Results and Discussion

4.1 Sensitivity Studies

The sensitivity studies can be divided into two types: 1) simulations where values of parameters affecting the structure of the heterogeneous transmissivity fields are varied, and 2) simulations for which values of parameters affecting drift are varied. Prior to providing detailed results of the sensitivity studies, a comparison of a set of simulations is discussed to elucidate the factors affecting mass-recovery rates for a single-porosity conceptualization of a SWIW test with plume drift.

4.1.1 Factors affecting mass-recovery rates

Two factors affect mass-recovery rates in a single-porosity system: 1) the amount of plume drift during the resting phase and 2) the structure of the heterogeneity relative to the location of the well.

Figure 3 illustrates how increases in plume drift (by increasing the resting-phase duration) in a heterogeneous system decrease the mass-recovery rates. This trend appears to be true regardless of the structure of the heterogeneous transmissivity field. In some circumstances, plume drift can lead to loss of mass. For the simulation with a 36-hour resting-phase duration shown in Figure 3b, approximately 1.5% of the mass is carried beyond the well's capture zone during the resting phase and is permanently lost. In another case (not shown), a gradient of 0.014 in a system with an advective porosity of 1×10^{-3} leads to mass loss as great as 18%. Clearly, steep gradients combined with low advective porosities can lead to significant mass loss beyond the capture zone of the withdrawal well.

For different transmissivity fields defined by the same variogram, mass-recovery rates can vary greatly (compare Figures 3a and b). In the case of Figure 3a, the early-time recovery curve is quite similar to the homogeneous case because the transmissivity field is relatively homogeneous in the region of the plume. In the other case (Figure 3b), recovery rates are significantly slower than those in a homogeneous transmissivity field.

The results of one flow and transport simulation (Figure 4) illustrate the process by which plume drift in a heterogeneous medium can result in decreased mass-recovery rates. The base-case transmissivity-field realization (Figure 4a) producing the slowest mass-recovery rate is chosen for this demonstration (the same simulation presented as the bold line in Figure 3b). The flow paths that dominate plume movement during the resting phase are those that carry the plume in a southeastern direction through high-transmissivity areas located both southeast and southwest of the well (Figure 4b). The shape of the plume after the resting phase illustrates the influence of these high-transmissivity regions (Figure 4c). During the withdrawal phase, the high flux (primary) flow paths to the well are from the southwest and southeast (Figure 4d). Tracer that is transported during the resting phase along the high transmissivity feature located southwest of the well must return to the well along lower flux (secondary) flow paths (Figure 4d). Transport along these secondary flow paths is through a lower transmissivity region. This new transport path causes the mass-recovery rate to be slower than if the transport paths had been reversible.

In summary, results of the simulation presented in Figure 4 suggest that if high-transmissivity areas are equally connected to the well by primary flow paths during the injection, resting, and withdrawal phases, then drift will have only a small effect on mass-recovery rates; the transport pathways are essentially reversible. In contrast, if, during the resting phase, tracer is

carried to regions where the most direct path during withdrawal is through a low-transmissivity area, mass-recovery rates will decrease significantly.

4.1.2 Heterogeneity

To understand the effects of heterogeneity on mass-recovery rates, several suites of simulations are conducted varying values of parameters that define the variograms and transmissivity frequency distributions. Parameter values for these sensitivity studies are summarized in Table 1. Given the large number of simulations, a simple metric is needed to compare results. Since our interest is primarily in late-time behavior, time to 90% mass recovery, as shown in Figure 3, is selected as the metric.

The parameter with the greatest effect on the mass-recovery rate is σ_{lnT} (Figure 5a). As σ_{lnT} increases, the rate of mass recovery decreases. This result is similar to that reported in *Tsang* [1995]. The larger the σ_{lnT}, the greater the degree of flow channeling. This channeling increases the likelihood that, during the resting phase, tracer will travel into or further within areas where the flux to the well is low during the withdrawal phase. As σ_{lnT} increases, the contrast in the magnitude of the transmissivity between the primary and secondary flow paths also increases. Larger contrasts in transmissivities (and fluxes) between primary and secondary flow paths result in the tracer being more easily diluted or trapped in lower transmissivity areas. All of these factors lead to reduced mass-recovery rates.

The spread of time to 90% mass recovery also increases as σ_{lnT} increases. For simulations that are highly heterogeneous in the vicinity of the solute plume (e.g. Figure 3b and Figure 4), an increase in σ_{lnT} leads to greater contrasts between high and low-transmissivity areas

leading to decreases in mass-recovery rates. However, for simulations that have relatively homogeneous transmissivites in the region of the plume (e.g. Figure 3a), mass-recovery rates do not change significantly with changing σlnT.

The results of simulations presented in Figure 5b suggest that the correlation length does not have a strong effect on mass recovery. If the correlation length is extremely large or small relative to the area occupied by the plume, mass-recovery rates are anticipated to be fast since the system will appear homogeneous in the area of interest. These sensitivity simulations investigate intermediate values of λ, which produce heterogeneous conditions in the vicinity of the plume. The results of the simulations indicate that there is not a critical correlation length that minimizes or maximizes mass-recovery rates. The range in mass-recovery rates is largest for a correlation length of 15 m, suggesting the possibility of a greater likelihood of slow mass-recovery rates for the 15-m correlation length. However, it appears that as long as the system is heterogeneous, the correlation length of the system plays a secondary role in controlling mass-recovery rates.

Simulations with bimodal and Gaussian distributions are compared to examine the effects of the shape of the transmissivity frequency distribution on mass-recovery rates (Figures 5c and d). The results show that, in most cases, mass-recovery rates, as defined by time to 99% mass recovery, are slower for simulations using the bimodal distribution as compared to simulations using the Gaussian distribution (Figure 5d). The slower mass-recovery rates for simulations using a bimodal distribution are explained by the higher probability that a low-transmissivity area is located between the tracer location at the end of the resting phase and the pumping well. This increased likelihood is due to there being regions of low transmissivity in the bimodal distribution and these regions tending to be well connected. However, it is not until very late times that the

mass-recovery rates are significantly slower for simulations using the bimodal distribution. If time to 90% mass recovery is used as a metric, there appears to be an equal probability that the mass-recovery rate will be slower when a bimodal distribution is used than when a Gaussian distribution is used.

4.1.3 Controls on plume drift

In addition to heterogeneity, the amount of plume drift strongly controls mass-recovery rates. Plume drift is primarily controlled by three factors: 1) porosity, 2) resting-phase duration, and 3) hydraulic gradient. From Darcy's law, the magnitude of plume drift is defined as:

$$Drift = \frac{T}{b\phi}\frac{dh}{dl}(t_r) \qquad (2)$$

where T is the mean transmissivity [L^2/T], b is the thickness of the transmissive layer [L], ϕ is the porosity [-], dh/dl is the regional gradient [L/L], and t_r is the resting-phase duration [T]. This definition is correct only for a homogeneous system, but can provide a good approximation of the relative magnitude of drift when heterogeneous systems are compared.

To examine the relative importance of the three variables controlling plume drift (porosity, gradient and resting-phase duration) in a heterogeneous system, four sets of simulations are run. For each set, the values of two of the three variables are varied in a coordinated fashion such that the expected plume drift, as calculated by Equation 2, remains constant. A comparison of the range in drift for the four sets of simulations shows that the amount of drift is approximately the same for the simulation sets [*Meigs et al.*, in review].

The results in Figure 6 show the relative effect of porosity, resting-phase duration, and gradient on mass-recovery rates for an expected constant drift distance. Regional gradient has a clear effect on the rates of mass recovery. The effect on mass-recovery rates is large for different porosities and gradients but the same resting-phase duration (compare sets A and B) and for different resting-phase durations and gradients but the same porosity (compare sets B, C, and D). As the magnitude of the regional gradient increases, the mass-recovery rates decrease and the range in mass-recovery rates increases. Variations in porosity and resting-phase duration, in contrast, do not appear to significantly affect mass-recovery rates. When porosity and resting-phase duration are varied but gradient is held constant, the effect on mass-recovery rates is small (compare sets A and C).

The regional gradient affects mass-recovery rates due to its potential ability to interfere with flow to the well during the withdrawal phase. Downgradient of the well, the flux to the well during withdrawal decreases as the gradient increases. Because a large percentage of tracer resides downgradient of the well at the end of the resting phase, this reduction in mass flux toward the well can have a strong effect on mass-recovery rates. The net effect is that, as the regional gradient increases, overall tracer flux to the well is reduced and mass-recovery rates decrease. In some cases, the gradient is large enough to carry a portion of the tracer outside the capture zone of the pumping well, which results in less than 100% mass recovery.

4.2 WIPP-specific simulations

The sensitivity studies provide insight into how model parameters representing characteristics of an aquifer and tracer test design affect mass-recovery rates in a single-porosity system. These insights are then used to determine whether observed mass-recovery rates from the

SWIW tracer tests conducted at the WIPP site could be explained with a single-porosity conceptualzation.

When the simulations for the H-11 and H-19 tests are compared, a much greater spread in mass-recovery rates is observed for H-11 conditions (Figure 7). The estimated porosity is higher and estimated gradient is lower at H-19 than at H-11. This combination of parameters at H-19 leads to simulations with significantly less drift and, therefore, less spread and faster mass-recovery rates than the H-11 simulations.

For the SWIW test conditions at the H-19 hydropad, single-porosity simulations produce recovery curves with longer times to peak concentration and higher peak concentrations than the observed test data (Figure 7a). Simulated mass recovery is much faster than observed mass recovery (Figure 7b). These results indicate that single-porosity simulations using realistic end-member parameter values cannot reproduce the observed data.

The results for H-11 simulations also show that the observed SWIW test data can not be matched with a single-porosity conceptualization (Figure 7c and d). For one transmissivity-field realization, the simulated mass and normalized concentration recovery curves are similar to the observed data up to approximately 100 hours into the test (Figure 7c and d). However, two important differences between the results of this simulation and the observed data at later times are noted. First, the slope of the simulated cumulative mass-recovery curve approaches zero between 400 and 500 hours into the test (Figure 7d). In contrast, the slope of the observed data remains positive, indicating continued mass recovery at these later times. In addition, simulated normalized concentrations decrease significantly relative to the data and fall outside the confidence limits of the data.

There are additional indications that a single-porosity conceptualization is not an appropriate model for both the H-11 and H-19 hydropads. The inability of the single-porosity model to match tracer data is consistent with hydraulic data at both hydropads, which require a double-porosity interpretation [*Beauheim*, 1989; *Beauheim and Ruskauff*, 1998]. In our attempt to be conservative, we were likely overconservative with the parameter with the most uncertainty: σ_{lnT}. Sensitivity studies show that if σ_{lnT} is decreased to 2.1, a value still thought to be conservative, the simulated results do not match the observed data at any time with the single-porosity conceptualization [*Meigs et al.*, in review].

Given the uncertainty in σ_{lnT}, note that the value used by *Lessoff and Konikow* [1997] is higher (by at least a factor of 2) than those reported from measurements (Table 3). The variance in logT used by *Lessoff and Konikow* [1997] is similar to the value calculated from hydraulic tests in the vicinity of the WIPP site (an approximately 700 km^2 area) (Table 3). The unrealistically large value used by *Lessoff and Konikow* [1997] could explain the gradual mass recovery and the multipeaked recovery curves of their simulations. Also of relevance in a comparison of our study to *Lessoff and Konikow* [1997] is the length of time over which the simulations are run. While a direct comparison is difficult, both parameters sets, based on WIPP-site data, are similar enough for a qualitative comparison. The *Lessoff and Konikow* [1997] simulations were run to less than 200 hours from time of injection. This short simulation time leads to ambiguous results for distinguishing between a single- and double-porosity conceptualization. It is predicted that if their simulations with slow mass-recovery rates had been continued to a later time, a single-porosity, heterogeneous system response would have been observed, i.e. less than 100% mass recovery as the slope of the mass-recovery curve approaches zero.

In addition to regional flow combined with aquifer heterogeneity, two other scenarios have been proposed that could cause gradual mass recovery without matrix diffusion. These two scenarios were investigated prior to running the WIPP-specific simulations and eliminated as explanations for gradual mass-recovery rates [*Meigs et al.*, in review]. The first scenario involves the loss of mass from the injection system to the bottom of the borehole during the tracer injection phase. During the withdrawal phase, this mass could diffuse back into the test interval, resulting in gradual mass recovery at late time. Even with conservative assumptions for diffusion rates and surface areas for diffusion, the amount of mass that could diffuse from the bottom of the borehole is very small and has an insignificant effect on the observed mass-recovery curves. The second scenario for gradual mass-recovery rates is tracer sorption to the aquifer materials. Simulations show that sorption results in relatively rapid mass recovery because it reduces the plume size and the ability of the regional flow field to transport the tracer during the resting phase.

In summary, the late-time data from the H-19 and H-11 SWIW tracer tests cannot be matched if a single-porosity conceptualization is assumed. This result suggests that diffusion is occurring in the aquifer and reinforces the value of collecting late-time data. However, the late-time slope of the observed data does not match the characteristic –1.5 slope predicted by a conventional double-porosity model, which assumes a single rate of matrix diffusion. The late-time slopes for the observed SWIW test data vary between –2.05 and –2.75. *Haggerty et al.* [this issue] show that a double-porosity model with multiple rates of diffusion provides an excellent explanation for the observed data, including the late-time slope.

5. Guidelines for Design and Interpretation of SWIW Tests

Single-well injection-withdrawal tracer tests provide an important tool for distinguishing between single- and double-porosity systems. To improve this tool, the insights gained from the results of the previously described simulations are examined to assist in test design and interpretation.

In designing a SWIW tracer test, the higher the pumping rate and the smaller the injection volume, the greater the likelihood of distinguishing between a single- and double-porosity conceptualization. Figure 8 presents a summary of the sensitivity studies that supports this point. The median time to 90% mass recovery for each set of 30 simulations is plotted versus the ratio of pumping rate (Q_p) to the background volumetric flow rate (Q_b). The background volumetric flow rate is defined as the volume of fluid that moves through the cross-sectional area of the tracer plume during the resting phase, assuming a homogeneous transmissivity field. This flow rate is dependent upon the injection volume, the porosity and the regional flow gradient. Assuming a specific location is being tested, no control over the regional gradient, porosity, or transmissivity of the system exists. Figure 8 illustrates that mass-recovery rates in a single-porosity system increase (time to 90% mass recovery decrease) logarithmically as Q_p/Q_b increases. Thus, in designing a SWIW tracer test, maximizing Q_p/Q_b (i.e maximizing pumping rate and/or minimizing injection volume) is advantageous to decreasing the effects of drift on mass-recovery rates. The decrease in volume minimizes the likelihood of channeling as shown in Figure 4. Figure 8 also illustrates that Q_p/Q_b decreases as resting-phase duration increases. Thus, as the resting-phase duration increases, an increasingly larger Q_p/Q_b is needed to minimize the effects of drift on mass-recovery rates.

In designing a SWIW test to evaluate whether the aquifer should be conceptualized as a single- or a double-porosity system, a careful balance must be struck between maximizing Q_p/Q_b and maximizing the likelihood of detecting diffusion. While the injection volume should be minimized to avoid confusion between a single- and double-porosity conceptualization, a sufficient amount of mass is needed to ensure good late-time data recovery. Furthermore, tests designed for the purpose of increasing the likelihood of detecting diffusion in an aquifer require slower pumping rates, greater volumes of tracer and greater resting-phase duration, all of which work against maximizing Q_p/Q_b. Calculations using a double-porosity conceptualization show that with significant diffusion rates, the likelihood of mass-recovery rates approaching those in a single-porosity system is minimal [*Meigs et al.*, in review]. However unlikely confusion between single- and double-porosity conceptualizations might be, pre-testing calculations should be performed to carefully optimize a SWIW test design.

Site-specific sensitivity analyses are recommended to design the optimal SWIW tracer test. In conducting these pre-test calculations, transmissivity fields that include anisotropy, if applicable, and with the largest reasonable σlnT should be generated. Transport simulations should be run using site-specific bounding parameters that maximize plume drift (i.e., largest gradient and smallest porosity). Breakthrough curves can be examined to determine the relationship between mass-recovery rates and plume drift. If the pre-test calculations indicate that reduced mass-recovery rates with a single-porosity conceptualization are likely, double-porosity simulations should be run for comparison.

Collection of adequate late-time data is usually critical for interpretation of SWIW tests. If drift is significant, some of the injected mass may be carried outside the withdrawal capture

zone (e.g., Figure 3b, 36-hour resting phase). Unrecoverable mass may be indicated by a derivative with respect to time of the late-time mass-recovery curve close to zero and a total cumulative mass less than 100%. Therefore, in examining tracer-test data, a total cumulative mass less than 100% (within measurement error) with a zero derivative could indicate a single-porosity system. In contrast, for a double-porosity system, a positive derivative at late times on the mass-recovery curve is expected if the mass has not traveled beyond the capture zone of the well. Selection of a tracer with adequate sensitivity and injection of sufficient mass such that the concentration of the recovered tracer spans several orders of magnitude is critical for the differentiation between a single- and double-porosity conceptualization.

6. Summary and Conclusions

Through numerical simulations, we have demonstrated how drift in a heterogeneous, single-porosity system affects mass-recovery rates for SWIW tracer tests. The insights are used to assess whether a single-porosity conceptual model in a heterogeneous system with plume drift can explain the data from SWIW tests at the WIPP site. The enhanced understanding of the effects of drift is also used to develop guidance for the design of SWIW tracer tests.

Site-specific factors that affect mass-recovery rates in SWIW tracer tests include structure of the heterogeneity, porosity, and regional gradient. In addition, design-controlled factors are resting-phase duration and injection volume. Of the factors affecting the heterogeneity structure, the magnitude of heterogeneity in the transmissivity field (as defined by $\sigma \ln T$) has the strongest influence on whether drift will result in reduced mass-recovery rates (as compared to the correlation length and frequency distribution model). The porosity, regional gradient, and resting-

phase duration affect mass-recovery rates because of their direct control on plume drift during the resting phase. Of these factors, the regional gradient has the largest impact on mass recovery because it potentially interferes with the pumping-induced fluxes toward the well during the withdrawal phase of the test. The smaller the injection volume, the less likely drift will affect mass-recovery rates because of reduced probability of channeling of the tracer.

Under the right conditions, a well-designed SWIW tracer test can be an excellent diagnostic tool for determining whether a single- or double-porosity conceptualization is appropriate. Tests conducted in areas with very steep gradients or tests with resting phases long enough to allow for extreme plume drift will not be effective because tracer will be carried beyond the capture zone established by pumping during the withdrawal phase. Even with full mass recovery, plume drift can redistribute the tracer such that the assumption of reversibility of flow paths is no longer true. Flow channeling can cause tracer to travel to areas with decreased fluxes towards the well during the withdrawal phase resulting in reduced mass-recovery rates. However, it appears that *extreme* heterogeneity and a rare configuration of the different transmissivity regions are required for drift to lead to gradual mass recovery without significant mass loss outside the capture zone of the well. The data compiled in Table 3 suggest that the high degree of heterogeneity required to create confusion between single- and double-porosity systems is rare at the SWIW tracer-test scale.

The observed data from the SWIW tracer tests at the H-11 and H-19 hydropads at the WIPP site cannot be matched assuming a single-porosity conceptualization. These results indicate that matrix diffusion is likely an important process in controlling slow mass-recovery rates observed in the WIPP test data. The late-time slope of the observed data is slightly steeper than

the -1.5 slope predicted by conventional double-porosity models. *Haggerty et al.* [this issue] demonstrate that a double-porosity model with multiple rates of diffusion can provide an excellent explanation for the observed data, including the late-time slope.

In designing a SWIW test and interpreting test results, precautions can be taken so as not to confuse a single-porosity system with a double-porosity system. The key in designing a SWIW tracer test is to allow for enough contact time and volume to maximize the likelihood of observing diffusion and, at the same time, minimizing the effects of drift. Site-specific pre-test simulations are recommended to optimize design parameters such as resting-phase duration, injection volume, and withdrawal pumping rate and to ensure field conditions will not result in extreme drift.

Collection of adequate late-time data can be critical for interpretation of SWIW tests. Late-time data are important for determining total mass recovery. Less than 100% mass recovery, within measurement error, along with a zero derivative with respect to time of the late-time normalized cumulative mass curve are indications that a single-porosity conceptualization of the system might be appropriate.

Acknowledgements

This paper was improved through the reviews of Peter Davies, Thomas Corbet, Vincent Tidwell, and Janet Chapman and discussions with Sean McKenna, Yvonne Tsang, and Roy Haggerty. Joanna Ogintz compiled the WIPP tracer-test data for use in this study. Yvonne Tsang conducted interpretive calculations that preceded and influenced the initial direction of this study. Sandia is a multiprogram laboratory operated by Sandia Corporation, a Lockheed Martin Company, for the United States Department of Energy under contract DE-AC04-94AL85000.

References

Abelin, H., L. Birgersson, L. Moreno, H. Widen, T. Agren, and I. Neretnieks, A large-scale flow and tracer experiment in granite, 2. Results and interpretation, *Water Resour. Res., 27(12)*, 3119-3135, 1991.

Ball, W. P., and P. V. Roberts, Long-term sorption of halogenated organic chemicals by aquifer material, 1. Equilibrium, *Environ. Sci. Technol., 25(7)*, 1223-1237, 1991.

Beauheim, R. L., Interpretations of single-well hydraulic tests conducted at and near the Waste Isolation Pilot Plant (WIPP) site, 1983-1987. *SAND87-0039*, Sandia Natl. Lab., Albuquerque, NM, December 1987.

Beauheim, R. L., Interpretation of H-11b4 hydraulic tests and the H-11 multipad pumping test of the Culebra dolomite at the Waste Isolation Pilot Plant (WIPP) site. *SAND89-0536*, Sandia Natl. Lab., Albuquerque, NM, September 1989.

Beauheim, R. L., L. C. Meigs, and P. B. Davies, Rationale for the H-19 and H-11 tracer tests at the WIPP site, *Field tracer experiments: Role in the prediction of radionuclide migration, synthesis and proceeding of an NEA/EC GEOTRAP Workshop*, Cologne, Germany, 28-30 August 1996, OECD/NEA, 107-118, 1997.

Beauheim, R. L., and G. J. Ruskauff, Analysis of hydraulic tests of the Culebra and Magenta dolomites and Dewey Lake Redbeds conducted at the Waste Isolation Pilot Plant site. *SAND98-0049*, Sandia Natl. Lab., Albuquerque, NM, January 1998.

Clauser, C., Permeability of crystalline rocks, *Eos Trans. AGU, 73(21)*, 233, 237-238, 1992.

Delhomme, J.P., Spatial variability and uncertainty in groundwater flow parameters: A geostatistical approach, *Water Resour. Res., 15(2)*, 269-280, 1979.

Deutsch, C. V., and A. G. Journel, GSLIB: Geostatistical software library and user's guide, 2nd ed., Oxford Univ. Press, New York, 1998.

Farnham, I. M., L. C. Meigs, M. E. Dominguez, K. Lindley, J. M. Daniels, and K. J. Stetzenbach, Fluoro- and chlorobenzoates as nonreactive tracers in groundwater, in review for submission to *Ground Water*.

Freeze, R. A., A stochastic-conceptual analysis of one-dimensional groundwater flow in nonuniform homogeneous media, *Water Resour. Res.*, 11(5), 725-741, 1975.

Gelhar, L. W., C. Welty, and K. R. Rehfeldt, A critical review of data on field-scale dispersion in aquifers, *Water Resour. Res., 28(7)*, 1955-1974, 1992.

Haggerty, R., S. W. Fleming, L. C. Meigs, and S. A. McKenna, Tracer tests in a fractured dolomite, 3. Analysis of mass transfer in single-well injection-withdrawal tests, *Water Resour. Res., this issue*.

Heer, W., and J. Hadermann, Grimsel test site, Modelling radionuclide migration field experiments. *PSI-Bericht Nr. 94-13*, Paul Scherrer Institute, Villigen, Switzerland, September 1994.

Holt, R. M., Conceptual model for transport processes in the Culebra Dolomite Member, Rustler Formation. *SAND97-0194*, Sandia Natl. Lab., Albuquerque, NM, August 1997.

Holt, R. M., and D. W. Powers, Geologic mapping of the Air Intake Shaft at the Waste Isolation Pilot Plant. *DOE-WIPP 90-051*, U.S. Department of Energy, WIPP Project Office, Carlsbad, NM, 1990.

Istok, J. D., M. D. Humphrey, M. H. Schroth, M. R. Hyman, and K. T. O'Reilly, Single-well, "push-pull" test for in situ determination of microbial activities, *Ground Water, 35(4)*, 619-631, 1997.

Jones, T. L., V. A. Kelley, J. F. Pickens, D. T. Upton, R. L. Beauheim, and P. B. Davies, Integration of interpretation results of tracer tests performed in the Culebra dolomite at the Waste Isolation Pilot Plant site. *SAND92-1579*, Sandia Natl. Lab., Albuquerque, NM, August 1992.

Leap, D. I., and P. G. Kaplan, A single-well tracing method for estimating regional advective velocity in a confined aquifer: Theory and preliminary laboratory verification, *Water Resour. Res., 24(7)*, 993-998,1988.

Lessoff, S. C., and L. F. Konikow, Ambiguity in measuring matrix diffusion with single-well injection/recovery tracer tests, *Ground Water, 35(1)*, 166-176, 1997.

Majoros, S., and H. A. Deans, Single-well chemical tracer tests since 1968. U.S. *Department of Energy Topical Report DOE/BC/20006-17*, U.S. Department of Energy, Washington, D.C., 1980.

McKenna, S. A., L. C. Meigs, and R. Haggerty, Tracer tests in a fractured dolomite, 4. Double porosity, multiple-rate mass transfer processes in two-well convergent-flow tests, *Water Resour. Res., this issue.*

Meigs, L. C., and R. L. Beauheim, Tracer tests in a fractured dolomite, 1. Experimental design and observed tracer recoveries, *Water Resour. Res., this issue.*

Meigs, L.C., S.A. McKenna, S. J. Altman, R. L. Beauheim, J. T. McCord, R. Haggerty, S. W. Fleming, T. L. Jones, J. Ogintz, and I. Farnham, Interpretations of tracer tests performed in the Culebra dolomite at the Waste Isolation Pilot Plant site, *SAND97-3109*, Sandia Natl. Lab., Albuquerque, NM, in review, expected publication 1999.

Mercer, J. W., and B. R. Orr, Interim data report on the geohydrology of the proposed Waste Isolation Pilot Plant site in southeastern New Mexico. *USGS Water Resour. Investigations Rpt.* 79-89, U.S. Geological Survey, Albuquerque, NM, 1979.

Moench, A. F., Convergent radial dispersion in a double-porosity aquifer with fracture skin: Analytical solution and application to a field experiment in fractured chalk, *Water Resour. Res.*, *31*(8), 1823-1835, 1995.

Moreno L., Y. W. Tsang, C. F. Tsang, F. V. Hale, and I. Neretnieks, Flow and transport in a single fracture: A stochastic model and its relation to some field observations, *Water Resour, Res.*, *24(12)*, 2033-2048, 1988.

Moreno, L., C. F. Tsang, Y. Tsang, and I. Neretnieks, Some anomalous features of flow and solute transport arising from fracture aperture variability, *Water Resour. Res.*, *26(10)*, 2377-2391, 1990.

National Research Council, Alternatives for groundwater cleanup, National Academy Press, Washington, D.C., 1994.

Seetharam, R. V., and H. A. Deans, CASTEM - A new automated parameter-estimation algorithm for single-well tracer tests, *Soc. Pet. Engr. Reservoir Engng.*, *4(1)*, 35-44, 1989.

Tomich, J. F., R. L. Dalton, Jr., H. A. Deans, and L. K. Shallenberger, Single-well tracer method to measure residual oil saturation, *J. Pet. Technol.*, *25(2)*, 211-218, 1973.

Tsang, Y. W., Study of alternative tracer tests in characterizing transport in fractured rocks, *Geophys. Res. Lett.*, *22(11)*, 1421-1424, 1995.

Tsang, Y.W., and C.F. Tsang, Particle tracking method for advective transport with diffusion into finite matrix blocks. *Report LBNL-42634*, E.O. Lawrence Berkeley Natl. Lab., Berkeley, CA, in review.

Volckaert, G., and A. Gautschi, Field tracer experiments in clay, *Field tracer experiments: Role in the prediction of radionuclide migration, synthesis and proceeding of an NEA/EC GEOTRAP Workshop*, Cologne, Germany, 28-30 August 1996, OECD/NEA, 95-101, 1997.

Wood, W. W., T. F. Kraemer, and P. P. Hearn, Intragranular diffusion: An important mechanism influencing solute transport in clastic aquifers?, *Science*, *247(4950)*, 1569-1572, 1990.

List of Figures

Table 1: Input parameters for the sensitivity study simulations.

	Base Case Value	Comparison Sensitivity Value(s) (— indicates no change from base case)
Mean transmissivity (T) (m^2/s)	5.10×10^{-5}	---
Standard deviation of lnT (σlnT)	1.76	0.88, 2.64, 3.52
Correlation length (λ) (m)	15	5, 25, 40
Transmissivity distribution	Gaussian	Bimodal
Culebra thickness (b) (m)	4.4	---
Porosity (ϕ)	1×10^{-3}	5×10^{-4}, 5×10^{-3}
Injection rate (m^3/s)	1.24×10^{-4}	---
Pumping rate (m^3/s)	2.23×10^{-4}	---
Regional gradient (dh/dl)	0.011	0.0011, 0.0027, 0.0054, 0.0081, 0.014, 0.0215
Mass of tracer injected (kg)	8.035	---
Tracer injection duration (sec)	8160	---
Chaser injection duration (sec)	15420	---
Resting-phase duration (sec)	63583	0,129600, 648000

Note: 30 realizations of transmissivity fields were generated and used in these simulations.

Table 2: Input parameters for the WIPP-specific simulations.

	H-11	H-19
Tracer	2,4-DCBA	2,4-DCBA
Mean transmissivity (T) (m^2/s)	5.10×10^{-5}	6.8×10^{-6}
Standard deviation of lnT (σlnT)	2.64	2.64
Correlation length (λ) (m)	15	15
Culebra thickness (b) (m)	4.4	4.4
Porosity (ϕ)	4×10^{-4}	6×10^{-3}
Injection rate (m^3/s)	1.24×10^{-4}	1.16×10^{-4}
Pumping rate (m^3/s)	2.23×10^{-4}	2.74×10^{-4}
Regional gradient (dh/dl)	5.7×10^{-3}	1.30×10^{-2}
Mass of tracer injected (kg)	8.035	4.995
Tracer injection duration (sec)	8160	7320
Chaser injection duration (sec)	15420	14580
Resting-phase duration (sec)	63583	63800

Note: 100 realizations of transmissivity fields were generated and used in these simulations.

Table 3: Comparison of ranges, standard deviations, and variances of permeabilities, hydraulic conductivities and transmissivities based on measurements reported in the literature and measurements made at the WIPP site to values used in the simulations for this study and the simulations by *Lessoff and Konikow* [1997].

	σlnT (m^2/sec)	**σlogK** (cm/sec)	**Variance logT** (m^2/sec)	**Range in k (m^2)** (Orders of magnitude - base 10)
σlnT = 0.88*	0.76 – 1.01 (0.86)	0.33 – 0.44 (0.37)	0.11 – 0.19 (0.14)	2.5 – 3.2 (2.8)
σlnT = 1.76*	1.51 – 2.01 (1.71)	0.66 – 0.87 (0.74)	0.43 – 0.76 (0.55)	5.1 – 6.4 (5.6)
σlnT = 2.64*	2.27 – 3.02 (2.57)	0.98 – 1.31 (1.12)	0.97 – 1.72 (1.24)	7.6 – 9.7 (8.3)
σlnT = 3.52*	3.02 – 4.02 (3.42)	1.31 – 1.75 (1.49)	1.72 – 3.05 (2.21)	10.1 – 12.9 (11.1)
Testing of the Culebra within the WIPP-site boundaries (41.4 km^2) [*Meigs et al.*, in review]	2.1	---	0.8	---
Testing of the Culebra within the vicinity of the WIPP site (~ 700 km^2) [*Meigs et al.*, in review]	3.3	---	2.0	---
Freeze [1975] Max reported (sandstone)	---	1.00	---	---
Freeze [1975] Min reported (sandstone)	---	0.20	---	---
Freeze [1975] Marly limestone	---	0.46	---	---
Freeze [1975] vuggy limestone	---	0.53	---	---
Delhomme [1979] Max. reported (Limestone)	---	---	0.98	---
Delhomme [1979] Min. reported (Limestone)	---	---	0.20	---
Clauser [1992] (maximum range - crystalline rocks)	---	---	---	8
Lessoff and Konikow [1997] (used in simulations)	---	---	2.0	---

* - Values reported are the minimum, maximum and median (in parentheses) for the 30 realizations where σlnT was set to the value indicated in the left-hand column for the *sgsim* simulations.

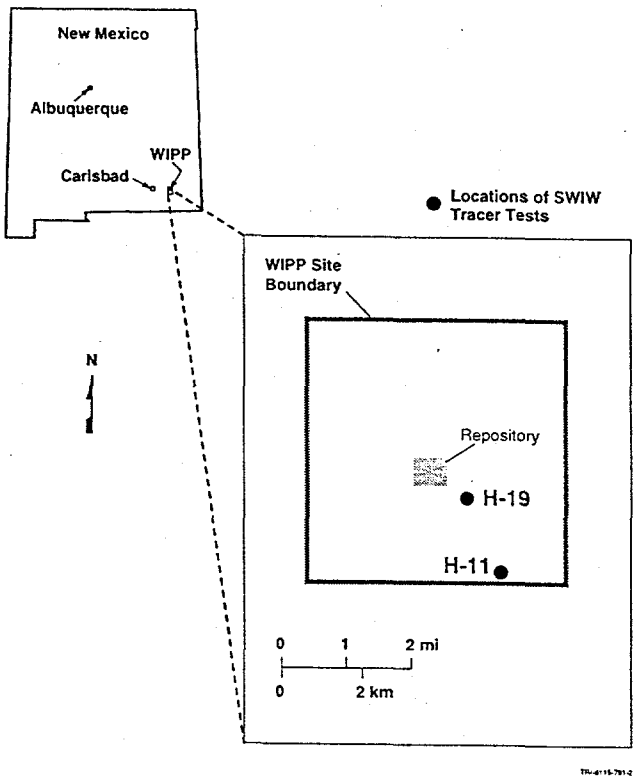
New Mexico
Albuquerque
WIPP
Carlsbad
Locations of SWIW Tracer Tests
WIPP Site Boundary
N
Repository
H-19
H-11
0 1 2 mi
0 2 km

Figure 1

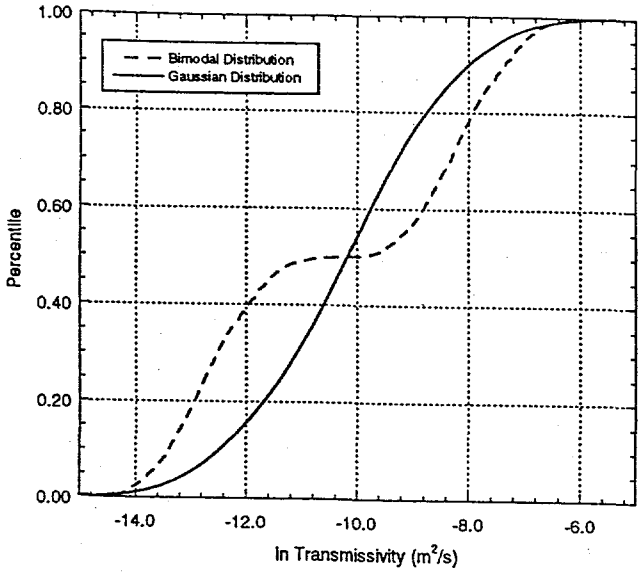
Bimodal Distribution
Gaussian Distribution
1.00
0.80
0.60
0.40
0.20
0.00
Percentile
-14.0
-12.0
-10.0
-8.0
-6.0
ln Transmissivity (m²/s)

Figure 2

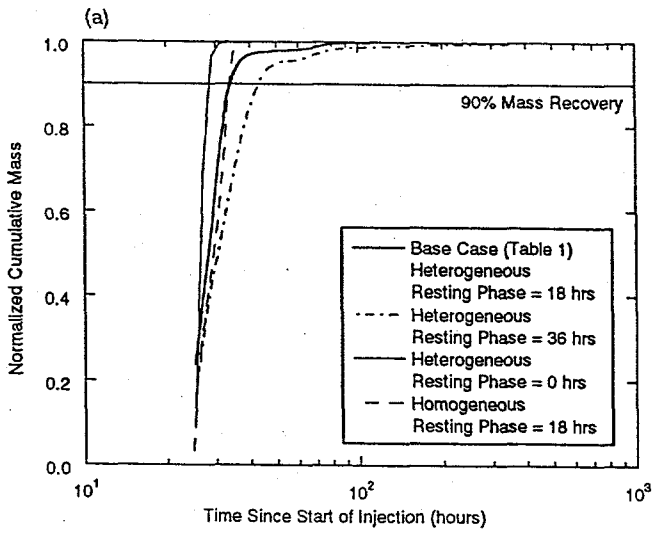
(a)
1.0
0.8
0.6
0.4
0.2
0.0
Normalized Cumulative Mass
90% Mass Recovery
Base Case (Table 1)
Heterogeneous
Resting Phase = 18 hrs
Heterogeneous
Resting Phase = 36 hrs
Heterogeneous
Resting Phase = 0 hrs
Homogeneous
Resting Phase = 18 hrs
10^1
10^2
10^3
Time Since Start of Injection (hours)

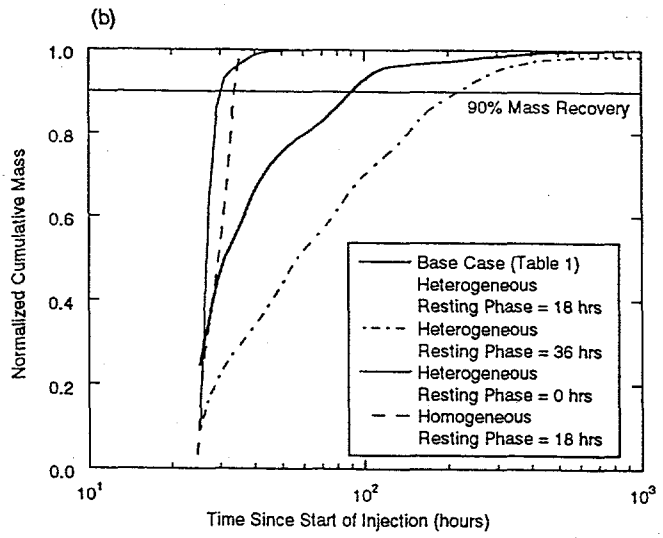
(b)
1.0
0.8
0.6
0.4
0.2
0.0
Normalized Cumulative Mass
90% Mass Recovery
Base Case (Table 1)
Heterogeneous
Resting Phase = 18 hrs
Heterogeneous
Resting Phase = 36 hrs
Heterogeneous
Resting Phase = 0 hrs
Homogeneous
Resting Phase = 18 hrs
10^1
10^2
10^3
Time Since Start of Injection (hours)

Figure 3

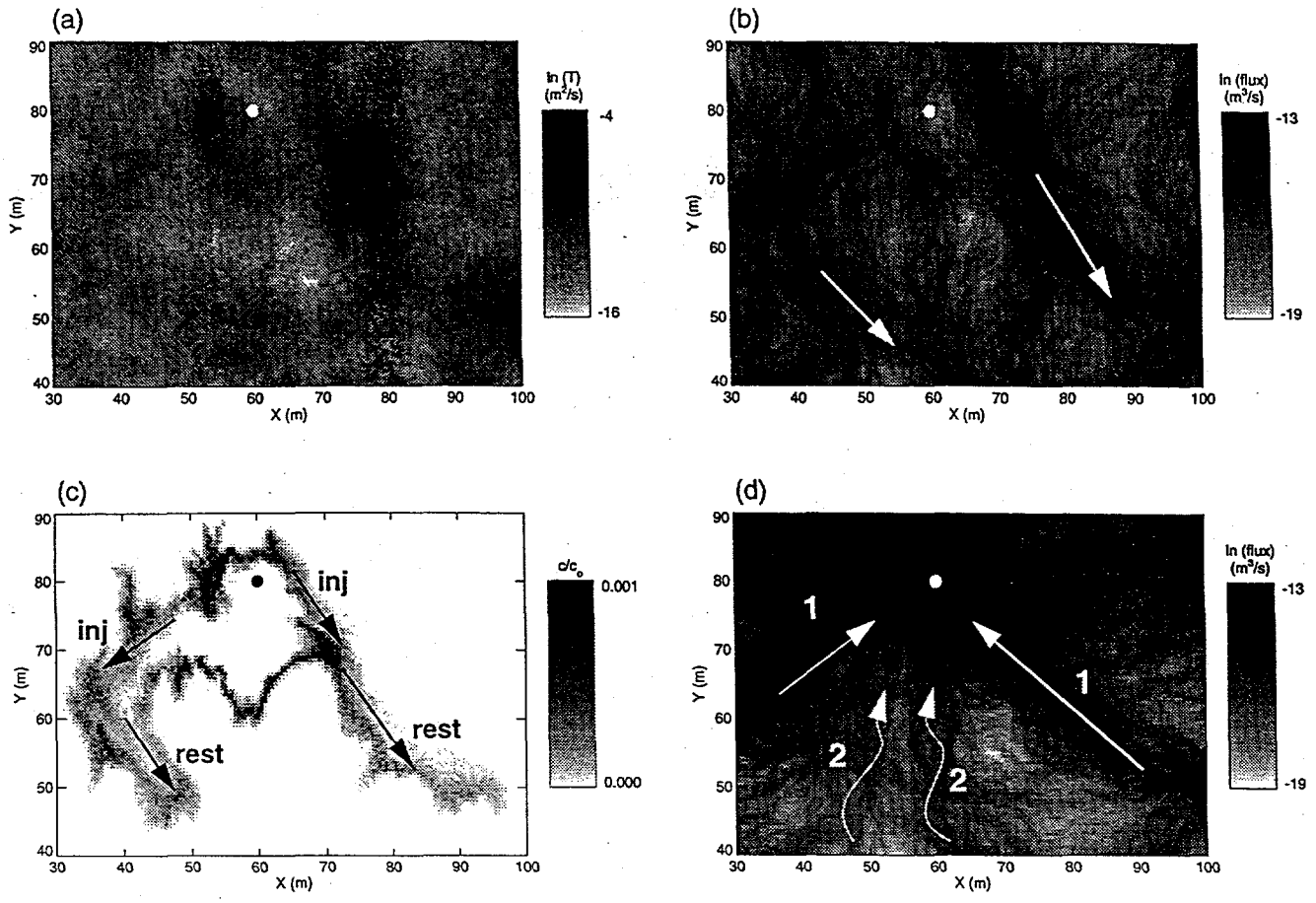
(a)
ln ∫T (m²/s)
-4
-16
Y (m)
X (m)
(b)
ln (flux) (m³/s)
-13
-19
Y (m)
X (m)
(c)
c/c₀
0.001
0.000
inj
inj
rest
rest
Y (m)
X (m)
(d)
ln (flux) (m³/s)
-13
-19
1
1
2
2
Y (m)
X (m)

Figure 4

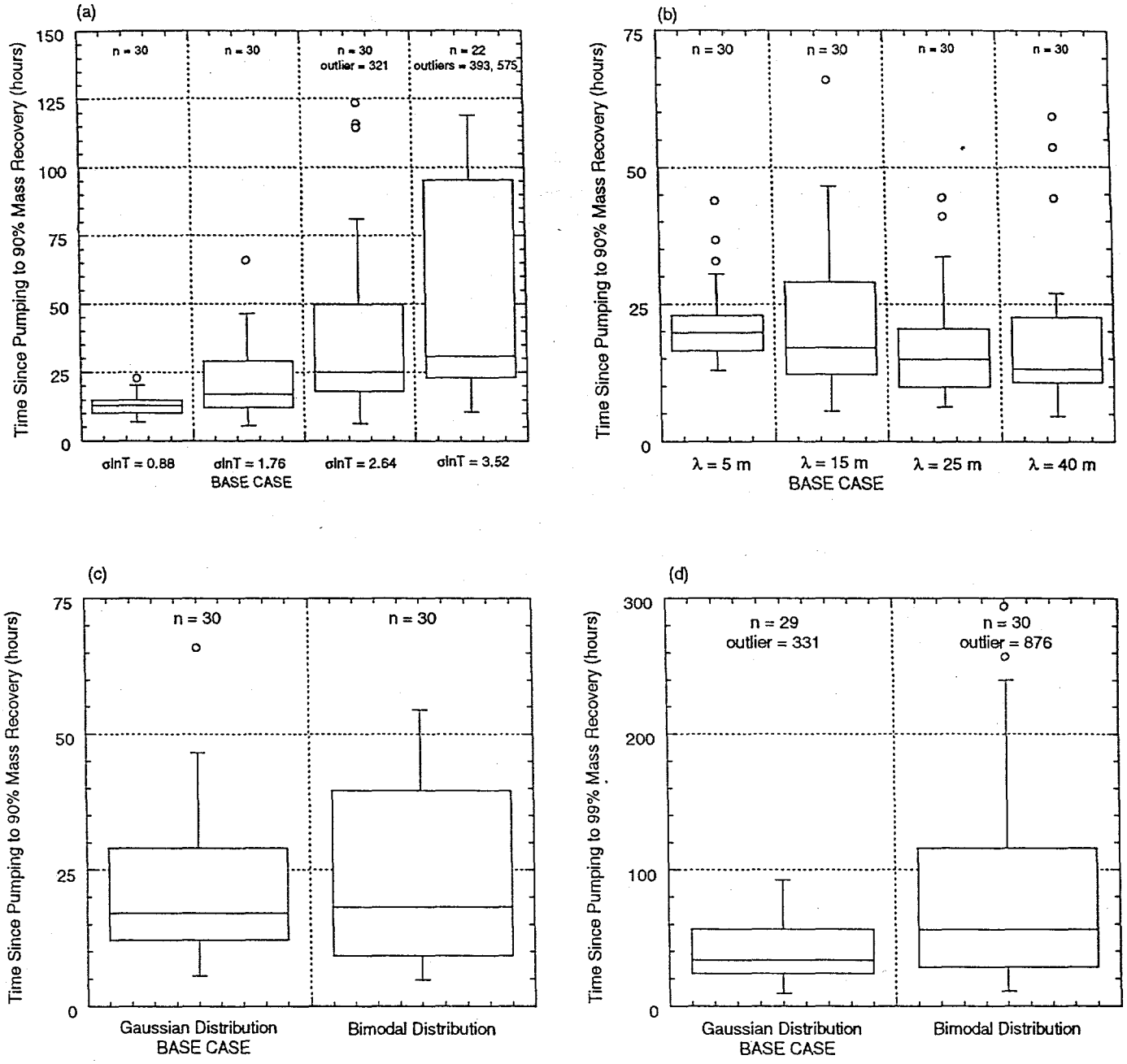
(a)
Time Since Pumping to 90% Mass Recovery (hours)
150
125
100
75
50
25
0
n = 30
n = 30
n = 30
outlier = 321
n = 22
outliers = 393, 575
σlnT = 0.88
σlnT = 1.76
BASE CASE
σlnT = 2.64
σlnT = 3.52
(b)
Time Since Pumping to 90% Mass Recovery (hours)
75
50
25
0
n = 30
n = 30
n = 30
n = 30
λ = 5 m
λ = 15 m
BASE CASE
λ = 25 m
λ = 40 m
(c)
Time Since Pumping to 90% Mass Recovery (hours)
75
50
25
0
n = 30
n = 30
Gaussian Distribution
BASE CASE
Bimodal Distribution
(d)
Time Since Pumping to 99% Mass Recovery (hours)
300
200
100
0
n = 29
outlier = 331
n = 30
outlier = 876
Gaussian Distribution
BASE CASE
Bimodal Distribution

Figure 5

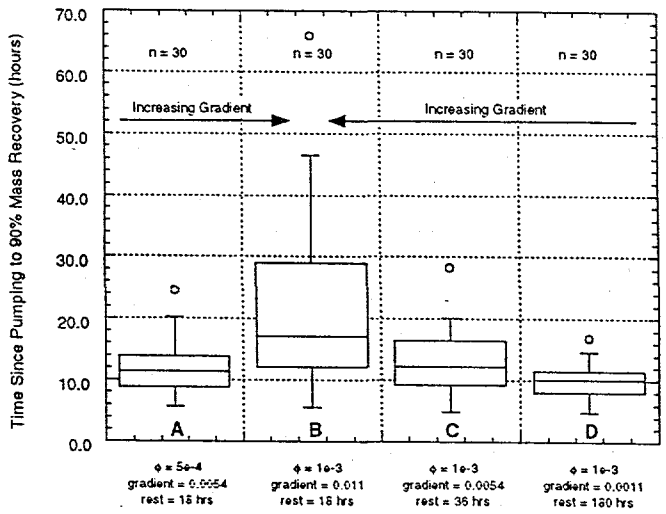
Time Since Pumping to 90% Mass Recovery (hours)
70.0
60.0
50.0
40.0
30.0
20.0
10.0
0.0
n = 30
n = 30
n = 30
n = 30
Increasing Gradient
Increasing Gradient
A
B
C
D
ϕ = 5e-4
gradient = 0.0054
rest = 18 hrs
ϕ = 1e-3
gradient = 0.011
rest = 18 hrs
ϕ = 1e-3
gradient = 0.0054
rest = 36 hrs
ϕ = 1e-3
gradient = 0.0011
rest = 180 hrs

Figure 6

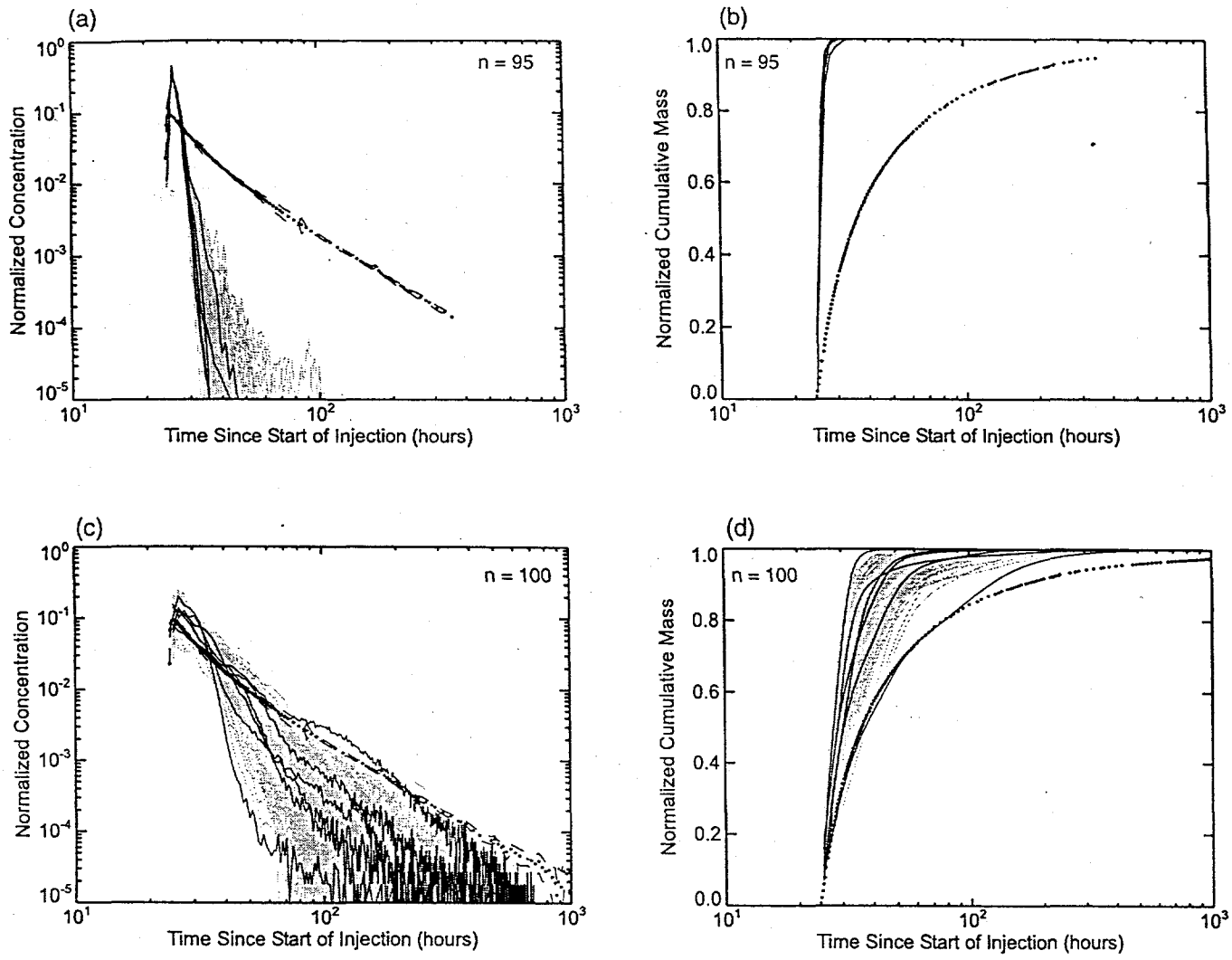
(a)
n = 95
Normalized Concentration
Time Since Start of Injection (hours)
(b)
n = 95
Normalized Cumulative Mass
Time Since Start of Injection (hours)
(c)
n = 100
Normalized Concentration
Time Since Start of Injection (hours)
(d)
n = 100
Normalized Cumulative Mass
Time Since Start of Injection (hours)

Figure 7

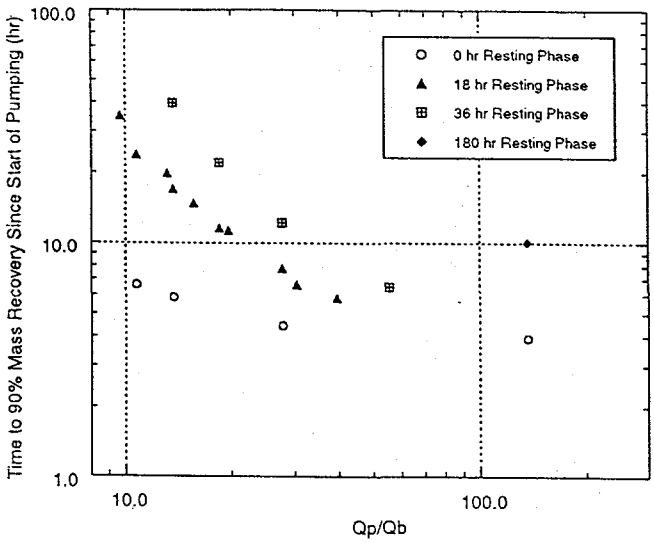
100.0
10.0
1.0
10.0
100.0
Qp/Qb
Time to 90% Mass Recovery Since Start of Pumping (hr)
0 hr Resting Phase
18 hr Resting Phase
36 hr Resting Phase
180 hr Resting Phase

Figure 8